RESEARCH PAPER

Plasma Time and Power Sequence Impact on Wettability Tuning and Mechanical Properties of Fluorinated Monolayer Graphene

Asieh Sadat Kazemi*, Fatemeh Bahar Azodzadegan, Seyed Mohamad Amin Tabatabee

* *asiehsadat_kazemi@iust.ac.ir*

Department of Physics, Iran University of Science and Technology, Tehran, Iran

Received: May 2025 **Revised: September 2025** **Accepted: September 2025**
DOI: 10.22068/ijmse.4004

Abstract: *Fluorinated graphene is an up-rising member of the graphene family and attracts significant attention since it is a 2D layer-structure, is self-lubricating, has a wide bandgap and high thermal and chemical stability. By adjusting the C–F bonding character and F/C ratios through controlled fluorination processes, fluorinated graphene can be utilized for a wide range of applications including energy conversion, storage devices, bio- and electrochemical sensors. Herein, monolayer CVD graphene/Cu was fluorinated via SF_6 plasma with a time and power sequence trial. Structural, morphological, roughness, adhesive forces, and wettability of fluorinated graphene were explored. Insight was gained by Raman spectroscopy, SEM and EDS, surface roughness and adhesive force measurements via AFM on different samples. Fluorination produced a p-doped structure, a blue shift in the 2D peak and a red shift in the D peak of the Raman spectra of graphene. Increasing plasma time increased the defects and weakened C-C bonds more rapidly at higher plasma power (40 W), whereas lower plasma power (15 W) retained more of the graphene properties (characterized by high La, LD, and low nD), as confirmed by Raman, SEM, and EDS analyses. Surface roughness and adhesive forces on the graphene surface mainly were increased with the increase in plasma time at a certain power. Higher plasma power resulted in more hydrophobic surfaces and even the wettability tuning occurred in the hydrophobic regime while lower plasma power demonstrated tuning in the hydrophilic regime. Influence of the underlying surface and π-electron pairs were shown to play more significant roles in tuning the wettability at higher plasma power.*

Keywords: *Graphene, Fluorination, Wettability, Raman, Surface roughness, Adhesive force.*

1. INTRODUCTION

Graphene, as the only carbonous surface with many remarkable electrical, optical, thermal, and mechanical properties, has been exploited for the fabrication of many biomedicine, bio-adhesion and bio-monitoring devices [1-3], desalination membranes [4-8], electric generators [9, 10], energy storage capacitors [11] and extraordinary wettable devices [12]. Graphene-related materials are promising solid lubricants due to the easy shear between lattice layers, but at the macroscale, their lubrication performance is mainly constrained by the external environment. Once fluorinated, they exhibit an excellent lubrication performance with a coefficient of friction more than half that of pristine graphene [13]. The surface energy of graphene governs fundamental interfacial interactions like molecular assembly, wetting, and doping [14]. A captive bubble measurement showed that large area free-standing clean graphene is hydrophilic with a contact angle of 42° ± 3° [15]. However, recent studies have shown a wide range of water contact angle (CA) on graphene [16, 17], with values ranging from 10° to 127° due to different aspects [18, 19]. Sample preparation and measurement conditions, adsorption of airborne hydrocarbons, cleanliness, and quality of the graphene–substrate and graphene–water interface all have substantial impacts on the measured CA [3]. Some of these aspects can be diminished by directing experiments in controlled atmospheres and by avoiding the use of polymers during the transfer process [20, 21].

Intrinsic hydrophilicity of graphene can be closely connected to the position of its Fermi level. The underlying substrate, or dopants, can tune hydrophilicity by modulating the Fermi level of graphene. By shifting the Fermi level of graphene away from its Dirac point, enhanced hydrophilicity has been shown with experiments and first-principles simulations [22]. Hydrogenating graphene raises its polar surface energy with little effect on its dispersive surface energy, leading to being more hydrophilic.

In contrast, fluorinating graphene lowers its dispersive surface energy with a substrate-dependent effect on its polar surface energy, which results in becoming more hydrophobic [14]. In a relevant study, the wettability of graphene patterned

[DOI: 10.22068/ijmse.4004]

into micro-scale sections without creating significant defects was investigated only by non-destructive hydrogen plasma. Hydrophobic graphene was progressively converted to hydrophilic hydrogenated graphene that reached superhydrophilicity. The stark contrast in the wettability of pristine and hydrogenated graphene allows selective positioning and isolating human breast cancer cells on arrays of micro-patterns [23]. Wetting behavior of CVD grown graphene, MoS_2 and WS_2 studied on few layers of h-BN and SiO_2/Si demonstrated a significant amount of influence by the underlying substrate due to dominant vdW forces. CA measurements indicated that graphene and graphene-like layered TMDs have dispersive surfaces with a dominating London-vdW force-mediated wettability [24]. Fluorographene is an exclusive functional material among vdW layered materials; the strong electronegativity difference between carbon and fluorine forms strong dipoles in the lattice [25], it preserves the original graphene lattice with a tunable carbon/fluorine stoichiometry [26] is one of the thinnest atomic dielectric materials with a high breakdown electric field of up to 10 MV/cm [27] and can decouple the long-range surface scattering in graphene transistors because of its excellent interfacial quality [28]. The application of this atomically thin layer into the synaptic junction region improves the efficiency, tunability, and symmetry of the synaptic plasticity and may be a promising building block for constructing efficient neuromorphic computing hardware [29, 30]. Among graphene functionalization methods [25, 56] plasma fluorination is compatible with conventional semiconductor processes and is highly efficient as it better controls the functionalization time and concentration of the functional groups and minimizes chemical residues [30-32].

Here, commercial monolayer CVD graphene on copper was fluorinated using SF_6 plasma at various plasma times and powers. Raman spectroscopy, AFM topography and force, SEM and EDS were conducted to characterize the as-grown graphene before and after fluorination while water CA measurements were used to demonstrate the distinct wettability behavior of the fluorinated surfaces. Mechanisms of wettability tuning via plasma time and power variation were discussed. Surface roughness and adhesive forces were also measured with fluorination time variation, aspects that are less studied in the literature, and insight was gained into their relationship.

2. EXPERIMENTAL PROCEDURES

2.1. CVD Graphene Fluorination

Chemical vapour deposited (CVD) graphene on Cu was purchased from Graphenea, without the polymeric coating. The thickness of the Cu was 18 μm. The large sheet was cut into several identical 0.64 cm^2 pieces, moved into a vacuum chamber, following [31, 56], exposed to SF_6 plasma and mildly fluorinated at two different plasma powers, P= 15 W and 40 W. At each power, plasma time sequence trials were conducted at T= 10, 20, 30, and 40 s. The processes are schematically shown in Figure 1. The fluorination time and power were based on effective values found in the literature [32, 49-52]. The time of fluorination was increased from 10 s to 40 s with 10 s steps at both 15 W and 40 W, and a 0 W-0 s sample was kept for comparison.

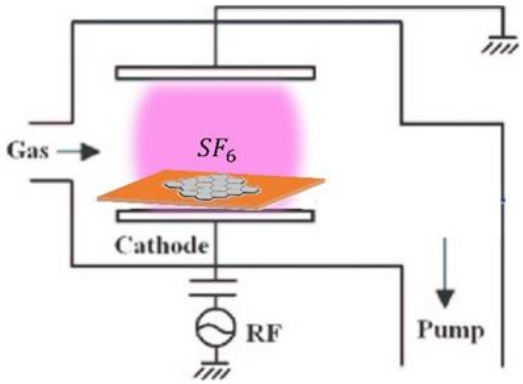

Fig. 1. Schematics of graphene fluorination via SF_6 plasma in an RF RIE setup under vacuum

2.2. Surface Topography, Roughness, and Force Measurements

Samples were imaged using an atomic force microscope (AFM, Ara Pajuhesh Advanced) in contact mode, and various surface roughness parameters were obtained via SPIP image processing software on images of 0-40 s fluorination time (and 40 W power) with identical scales. Furthermore, force spectroscopy measurements were performed on comparable regions in contact mode.

2.3. Water CA Measurements

Various methods are often used for measuring the CA of surfaces. Most of these techniques rely on

[DOI: 10.22068/ijmse.4004]

static contact angle measurements, while some involve measurement of advancing and receding contact angles [33-36]. For a surface with a global energy minimum, static CA is sufficient to give information on the wettability of the surface [35]. Here, the Sessile drop method was used to obtain water CA on 0 s-40 s fluorinated samples at both fluorination powers (15 W and 40 W), via a home-made CA instrument equipped with a digital camera. In this method, 0.1 ml of distilled water was dropped with a precise micropipette on the surface of the samples. Immediately, 240 s length video was captured from graphene surface with a high-resolution camera. Using an image processing program (Image J), solid-liquid angles with an interval of 20 s were obtained for each sample. Measurements were iterated a second round after 48 h, and the average values were reported.

2.4. Raman Spectroscopy, SEM Imaging and EDS Measurement

Raman spectra of pristine graphene and fluorinated samples were taken on four random points by a TEKSAN instrument with a laser excitation of 532 nm. The average values of the measurements were reported for each fluorination time. Scanning electron microscopy (SEM) was performed on different samples with a Vega Tescan instrument via backscattered electrons (BSE) imaging and a WD of about 15 mm. An energy dispersive spectrometer (EDS) with the same instrument was used for elemental analysis on the surface of graphene samples.

3. RESULTS AND DISCUSSION

3.1. Roughness and Force Measurement Insights on Fluorinated Graphene

Atomic force microscopy images were recorded on identical image windows $10\ \mu m^2 \times 10\ \mu m^2$ on graphene surfaces at 0 s–40 s fluorinated samples exposed to 40W SF_6 plasma (Figure 2a). For better comparison, various roughness parameters were extracted from topographic images by SPIP image processing software (Figure 2b). Average roughness (Sa) and root mean square roughness (Sq) are the average of the deviations from the mean plane and the standard deviation of the height distribution, respectively. Skewness (Ssk) measures deviations relative to the normal height, and Kurtosis (Sku) measures "tailedness" of the distribution. For Ssk< 0, there is a prevalence of valleys, and for Ssk >0, a prevalence of peaks occurs. For Sku< 3, there is a prevalence of high peaks and/or low valleys, whereas in Sku >3, there is a lack of peaks and/or valleys. As seen, Sa and Sq both increase with the increase in fluorination time due to the rise of defective structure of the graphene surface. At 0 s, these roughness values are around 22 and 27 nm, which is relatively high. This is due to the roughness of the underlying copper surface. Strikingly, at 30 s, these values are the highest, which may relate to the onset of copper fluorination explained in section 3.4 via the EDS results and discussions. Beyond 30 s, the fluorinated copper surface may have reoriented and induced lower roughness values. Ssk values for all fluorination times apart from 10 s, are above zero and indicate prevalence of peaks. In 10 s fluorinated graphene, with Ssk< 0, there is a prevalence of valleys. As of Sku, 0 s and 30 s samples exhibit a prevalence of high peaks and/or low valleys, whereas other samples lack peaks and/or valleys, with 10 s, 20 s, and 40 s samples lacking the most, respectively. AFM roughness measurements in [26] showed that doped and undoped graphene over flat surfaces have similar roughness, with Sq values of less than 10 nm.

Using AFM contact mode and a sharp contact tip, force spectroscopy measurements with 1000 nm indentation were carried out on identical image windows $10\ \mu m \times 10\ \mu m$ on graphene surfaces at 0 s–40 s fluorinated samples at 40 W SF_6 plasma (Figure 2c). To the best of our knowledge, roughness and force studies have not been conducted on fluorinated monolayer CVD graphene. The difference in force in the approach and retraction of the probe toward and from the graphene surface represents the adhesion force. At each point, 10 measurements were taken, and the average is presented for clarity. Interestingly, with the increase in fluorination time from 0 s to 10 s, the adhesive force on the surface increases from 21.72 nN to 29.03 nN. However, in agreement with the roughness data, the force drops to 26.70 nN at 20 s and further increases to 54.99 nN at 30 s. This is the highest force measured among fluorination times, while at 40 s, the force decreases to 47.31 nN. The area of the triangle formed in the force curves, gives an estimation of the work done by the adhesive force. A preliminary examination of these areas reveals a higher workload at higher fluorination times.

[DOI: 10.22068/ijmse.4004]

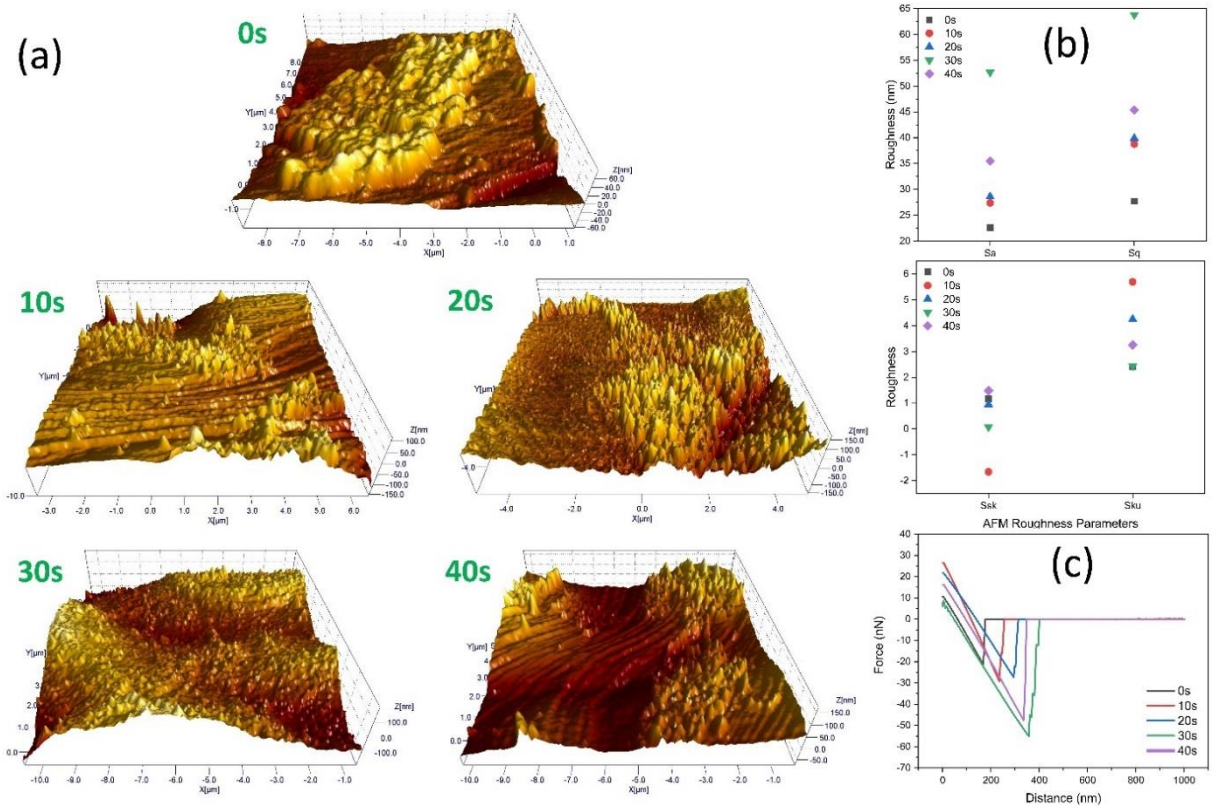

Fig. 2. a) 3D AFM topography images of 0 s-40 s fluorinated graphene exposed to 40 W SF_6 plasma, b) Comparison of roughness parameters with fluorination time; roughness data extracted from AFM topography images of 0 s-40 s fluorinated graphene exposed to 40 W SF_6 plasma, c) Evolution of force curves of 0 s-40 s fluorinated graphene exposed to 40 W SF_6 plasma

In [55], a substrate doping-induced charge carrier density modulation led to tunable adhesion of graphene. Therein, adhesion force measurements using an AFM probe revealed enhanced attraction toward undoped graphene. Adhesion force measurement of graphene/SiO_2 samples demonstrated ~25 nN, [55] comparable to the force measured in this work over 40 W 20 s graphene samples. In [26], an AFM tip was positioned above the center of a fluorographene membrane and indented it. The bending of the AFM cantilever as a function of its displacement, and the force acting on the membrane, was calculated from the cantilever's rigidity. Young's modulus obtained from analysis of the force-displacement curves showed fluorographene was three times less stiff than graphene, but still extremely high in comparison with structural steel [57]. Longer sp^3-type bonding in fluorographene results in a reduction in stiffness and breaking strength of the sheet [26].

3.2. Wettability tuning of Fluorinated Graphene

Understanding the wettability of 2D materials involves crucial steps to quantify the interplay between interfacial forces and the impact of water-surface, water-medium, and medium-surface interactions. It is shown that the intrinsic hydrophilicity of graphene can be intimately connected to the position of its Fermi level [59]. Graphene interacts with external molecules in its close vicinity through delocalized π-electrons. Recent studies have suggested that doping and charge injection into graphene can lead to higher water adsorption and changes in wettability [55, 58-60] while water is an electron acceptor. The interaction of graphene with atoms and molecules attracts great attention due to its potential applications when supported on a substrate, as opposed to its use in free-standing form. These applications include catalysis, photocatalysis, and gas sensing [60].

In an interesting study, electroplated Cu was used for in-situ CVD growth of graphene such that the graphene coating was well-adhered to the surface and followed the contours of the surface [61]. An outstanding anti-corrosion and wetting stability

[DOI: 10.22068/ijmse.4004]

was gained for the underlying surface, namely as a condensation surface for water harvesting [61]. Measurements of CA across fluorinated graphene bring insight into its wettability properties. A. Asharaf et al. [55] demonstrated that n-doped graphene is more hydrophobic while p-doped graphene is more hydrophilic with respect to undoped graphene. They demonstrated graphene's water CA changes by as much as 13° because of a 300 meV change in doping level. These results agreed with those attained by [59].

Here, a direct measurement method of the tangent angle at the three-phase contact point on a sessile drop profile was performed on the as-grown graphene on copper. Although graphene can be transferred to any substrate, unintentional contaminations, mainly polymer residue, are experimentally unavoidable, which totally hinders wettability investigations [59]. Since the main polymer used in CVD graphene transfer is polymethyl methacrylate (PMMA), the residues contain PMMA fragments, oxidized PMMA, short-chain hydrocarbons, crosslinked carbonaceous remainders and residual Fe^{3+} or Fe^{2+} from the $FeCl_3$ etching process [62-64]. These include C-C (sp^3), C-H, O-CH_3 and O-C=O. During transfer, water layers get trapped between graphene and the target substrate, where they act as nucleation sites for further contamination adsorption, such as hydrated salts [65]. Airborne or environmental adsorbates, such as hydrocarbons from lab air, oxygen, and ambient organic molecules, are other possible residues left on the graphene surface [66]. However, these contaminations are avoided here by avoiding transfer over a substrate. 0 s graphene samples presented CA just below 80° (Figure 3).

Studies show that graphene grown via the CVD method on copper substrate is hydrophilic, while its CA varies in different reports from around 60° to 85° [13, 16, 31]. A captive bubble measurement shows that free-standing clean graphene has a contact angle of ~42° [15]. With 15 W SF_6 plasma, at all fluorination times (10 s-40 s), the surface becomes more hydrophilic with the lowest CA measured for 30 s fluorination. This is in agreement with p-doped graphene wettability behaviour and the blue shift in the 2D band of Raman spectra. At 40 s, graphene becomes more hydrophobic, which may relate to the saturation of carbon atoms and the onset of copper fluorination or a reorientation of the surface. With 40 W exposure of SF_6 plasma, at most fluorination times (10 s, 30 s, 40 s), the surface becomes more hydrophobic with the highest CA measured for 30 s fluorination. At 40 s, graphene becomes more hydrophilic compared to 30 s, but remains hydrophobic compared to the 0 s sample.

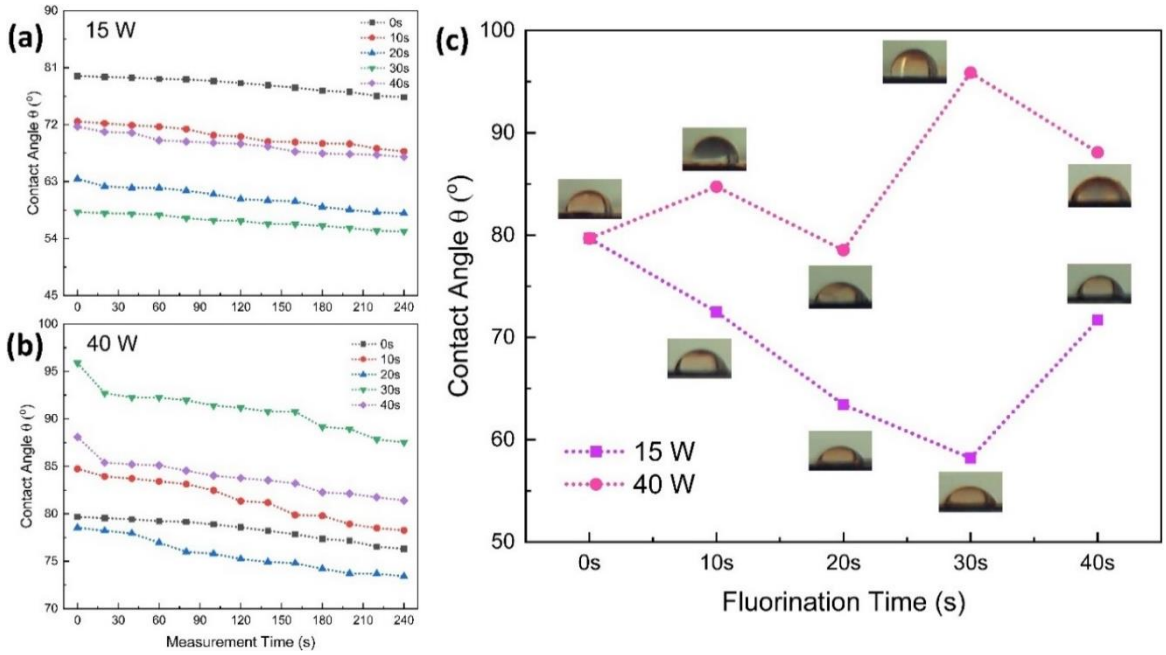

Fig. 3. Water contact angle measurement results on of 0 s-40 s fluorinated graphene at a) 15 W and b) 40 W SF_6 plasma in 240 s measurement time, c) comparison of contact angles at 0 s-40 s fluorination time in a single measurement time

[DOI: 10.22068/ijmse.4004]

The variations of CA with fluorination time exhibit the potential for wettability tuning. CA in all samples slowly declines in the 240 s period, which agrees with previous studies [13, 16, 31, 24, 58-61]. This is due to longer interaction times of the fluorinated graphene surface with water molecules and the higher chances for hydrogen bonding occurrence.

Figure 3(c) summarizes results on 0 s-40 s fluorination at both plasma powers at the beginning of the measurements. In 40 W graphene samples. Aromatic graphene rings with one or more fluorine atoms lose electrons, resulting in a loss of electron density that provides an opportunity for π-electron pair formation between oxygens in water and the rings. A few studies [67, 68] have investigated graphene saturation and its impact on hydrophobicity. At 40 s, water curvature resembles that in the 10s sample, indicating a reduction in hydrophilic nature. This may be due to the deformation of aromatic rings and the lower chance of water molecules forming π-electron pairs with the rings. The lower the plasma power, the more fluorine atoms that can sit on the carbon surface, and higher persistence of π-electron pairs happens. With the increase in plasma power, more of the carbon atoms become saturated.

Many studies have considered the wettability of polymer-assisted transferred monolayer CVD graphene and obtained CAs of ~81°, 79°, 33°, 78°, 48° over SiO_2, h-BN, Si, Au, glass, respectively [55, 24, 16]. However, only a few studies in the literature have investigated the wettability of monolayer CVD graphene directly on Cu without transfer and obtained CAs of ~80° and 86° [59, 16, 61]. Even fewer research investigated the impact of fluorination on the wettability of monolayer CVD graphene. T. Lim et al. [32] treated graphene by CF_4 plasma and attained CA ~104.9° of fluorinated graphene/SiO_2 at 50 W 20 s while CA of graphene/SiO_2 was ~66.7° for pristine graphene [32]. In another study, 4 min fluorination of monolayer graphene on Cu increased CA to ~95° from ~80° without fluorination.

Although several studies discussed the impact of the underlying substrate or the effect of the number of graphene layers on CA [15, 16, 55, 61], to the best of our knowledge, the effect of temperature variation on CA measurements has not been investigated on fluorinated graphene yet. However, research on graphene [69] confirms that temperature varying between 2°C and 90° can significantly influence its wettability by raising or lowering contact angles depending on the crystal orientation of the Cu surface during the graphene growth procedure. Therein, the lowest contact angle was obtained on graphene coating on copper with orientation (1 1 1). Defects on the surface of the Cu substrate were also impactful in a change in the wettability of the graphene layer. According to wetting theory [70], the equilibrium CA depends on surface tensions, which generally decrease with temperature. Fluorination changes graphene surface roughness, induces a band gap in the electronic band structure and more defects on the surface (see section 3.3), exhibits lower surface energy, and at elevated temperatures, thermal motions may enhance CA hysteresis and perturb wettability even more. At some higher temperatures (above 500°C), the fluorination may overturn, and the graphene sheet may lose most of its bonds with fluorine. For all these complex concerns, an in-depth study needs to be performed to understand microscopic impacts of wettability with the changes in temperature on fluorinated graphene at different regimes.

3.3. Raman Spectroscopy on Fluorinated Graphene

Raman spectroscopy of graphene confirms its typical characteristics with D-band (~1350 cm^{-1}), G-band (~1580 cm^{-1}), and 2D-band (~2690 cm^{-1}) [37]. This a very sensitive, powerful, and nondestructive technique to electronic structure and for the characterization of carbon-based materials including graphene [38, 39]. D-band indicates the presence of defects or other impurities, G-band corresponds to the tangential stretching mode of an ordered graphite structure with sp^2 hybridization (=C-), and 2D-band in graphene gives information about the degree of crystallinity and about the number of graphene layers [40-42]. With fluorination in graphene, =C- turn into -CF- in the bulk and -CF_2- at the edges. Figure 4(a) demonstrates Raman spectra of graphene at various fluorination time when exposed to 15 W and 40 W SF_6 plasma, respectively.

In each set of samples, an increase in fluorination time declines the intensity of the 2D peak and rises the D peak, significantly. There is also a red shift in the D peak while a blue shift occurs with the increase in fluorination time and power in agreement with [53]. The blue shift of the 2D peak is often related to hole doping, increase in

[DOI: 10.22068/ijmse.4004]

the number of layers, decrease in temperature, and decrease in strain and tensile strength [16, 43-48]. Here, the blue shift is mainly related to the exchange of aromatic C=C sp^2 hybridization with CF-CF sp^3 hybridization due to increase in fluorination time and power as seen in Figures 4(b,c). G peak position does not seem to change with the fluorination conditions and its intensity variations with fluorination time is not very significant. Figure 4(c) depicts 2D peak frequency increase with the increase in fluorination time for both powers in graphene samples. However, in 15 W, the increase in frequency is very fast while in 40 W is monotonic. Quantifying defects in graphene is another vital step toward describing fluorination [42]. The first-order Raman scattering process causes the G peak; a high-frequency E2g Raman allowed optical phonon, and it is characteristic of sp^2 hybridization. The D peak reflects a common feature of defect density in the graphene, assigned to an A_{1g} breathing mode at the Brillouin Zone boundary K [40, 41]. Figures 5(a,b) compare I_D/I_G and I_{2D}/I_G at different fluorination times and power. I_D/I_G at 0s fluorination in both sets of samples is approximately 0.2. However, with increased fluorination time, the D band intensity increases gradually in 15 W samples but more severely in 40 W samples up to 20 s, after which it increases much more slowly. On the contrary, I_{2D}/I_G, decreases fast with the increase in fluorination time in 15 W samples from 1.34 at 0 s to around 0.65 at 40 s. 40 W samples experience a fast decline in this ratio within the first 10 s of the fluorinations, but beyond this time, the probability of graphene saturation increases, and the I_{2D}/I_G ratio remains around 1 up to 30 s. With further increase of fluorination time to 40 s, this ratio drops to around 0.75, confirming an increase of defects in the graphene structure.

The ratio of the D to G intensities is shown to vary inversely with L_a known as the crystallite size, domain size or the in-plane correlation length [40-42]. Recent studies show that L_a can be estimated by Raman spectroscopy through the following relation:

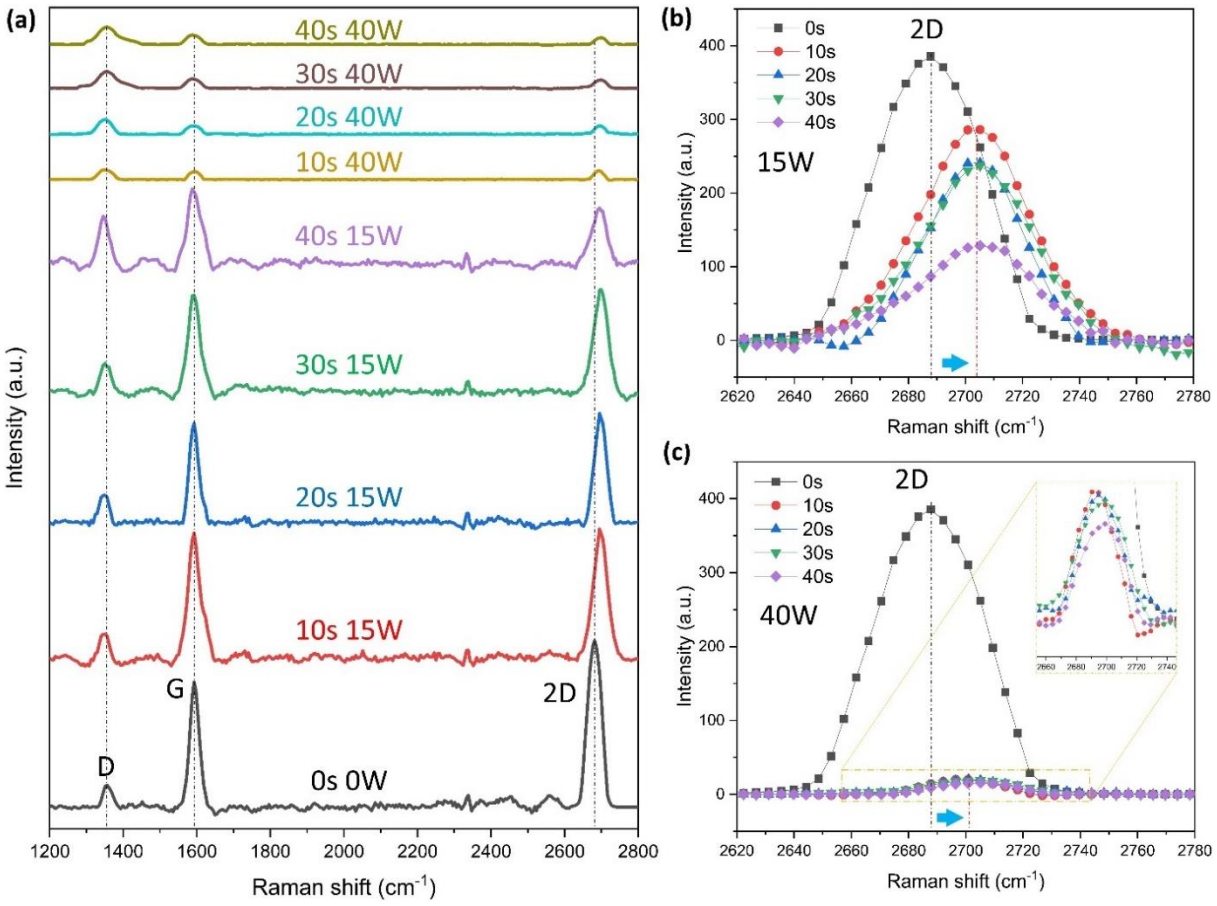

Fig. 4. Raman spectra a) of graphene at 0 s-40 s fluorination with 15 W and at 0 s-40 s fluorination 40 W SF_6 plasma exposure, b, c) showing blue shift of the 2D peak in both 15 W and 40 W fluorinated graphene samples

[DOI: 10.22068/ijmse.4004]

$$L_a = C(\lambda_L)\frac{I_G}{I_D} \quad (1)$$

Where $C(\lambda) = C_0 + \lambda_L C_1$. According to [41], C_0= -12.6 nm, C_1= 0.033 and λ_L is the excitation laser wavelength (532 nm in this work) [42]. L_a values for 0 s-40 s fluorination at 15 W and 40 W are compared in Figure 5(b) and Table 1. L_a as the domain size, is largest (about 28 nm) in graphene with 0 s 0 W fluorination in agreement with the literature [39]. With the increase in fluorination time at 15 W, L_a almost monotonically reduces from 0 s to 40 s, but at 40 W, it drastically decreases from 0 s to 10 s and slowly declines from 20 s to 40 s due to the increase in surface defects (Figure 5(d)). This quantity is in close relation with defect distance (L_D), through [42]:

$$L_D^2(nm^2) = (1.8 \pm 0.5) \times 10^{-9} \lambda_L^4 \frac{I_G}{I_D} \quad (2)$$

Therefore, when L_a decreases, the distance between defects also decreases with similar trend (Figure 5(e)). L_D is also related to defect density $n_D(\frac{1}{cm^2}) = \frac{10^{14}}{\pi L_D^2}$ [42] where:

$$n_D\left(\frac{1}{cm^2}\right) = (1.8 \pm 0.5) \times 10^{22} \frac{1}{\lambda_L^4}\left(\frac{I_D}{I_G}\right) \quad (3)$$

From the equations, it is expected that n_D will increase with the decrease in L_a and L_D. This can be seen in Figure 5(f) where n_D increase almost monotonically from 0 s to 40 s at 15 W fluorination while it increases much faster from 0 s to 10 s at 40 W fluorination. For simplicity of the discussion, average values of L_D and n_D are calculated and reported here. $I_{G/D}$ decrease and $I_{G/2D}$ increase with the increase in plasma time in this work agreed with the relevant studies in the literature on monolayer CVD graphene [26, 29, 32, 49, 51, 52, 54]. Even though the plasma treatment here was conducted without any filters over graphene, $I_{G/D}$, $I_{G/2D}$, L_a and L_D obtained with 40 W plasma here were comparable with those who applied filters and fluorination was conducted indirectly [29, 30, 52]. This suggests that even direct fluorination on graphene surface with controlled power and time of the plasma retains graphene's properties at an acceptable degree. All $I_{G/D}$, $I_{G/2D}$, L_a and L_D values obtained for 15 W plasma here were higher than those who used filters during plasma or had examined similar time and power of plasma. n_D values for different plasma time at 15 W plasma here were three orders of magnitude lower than the literature (Table 1). The significantly lower n_D and higher L_a and L_D values obtained in this work can be attributed to the direct plasma treatment of as-grown graphene/Cu, a method not commonly used in the literature, where monolayer CVD graphene is typically transferred onto another substrate, such as SiO_2/Si, using a polymer.

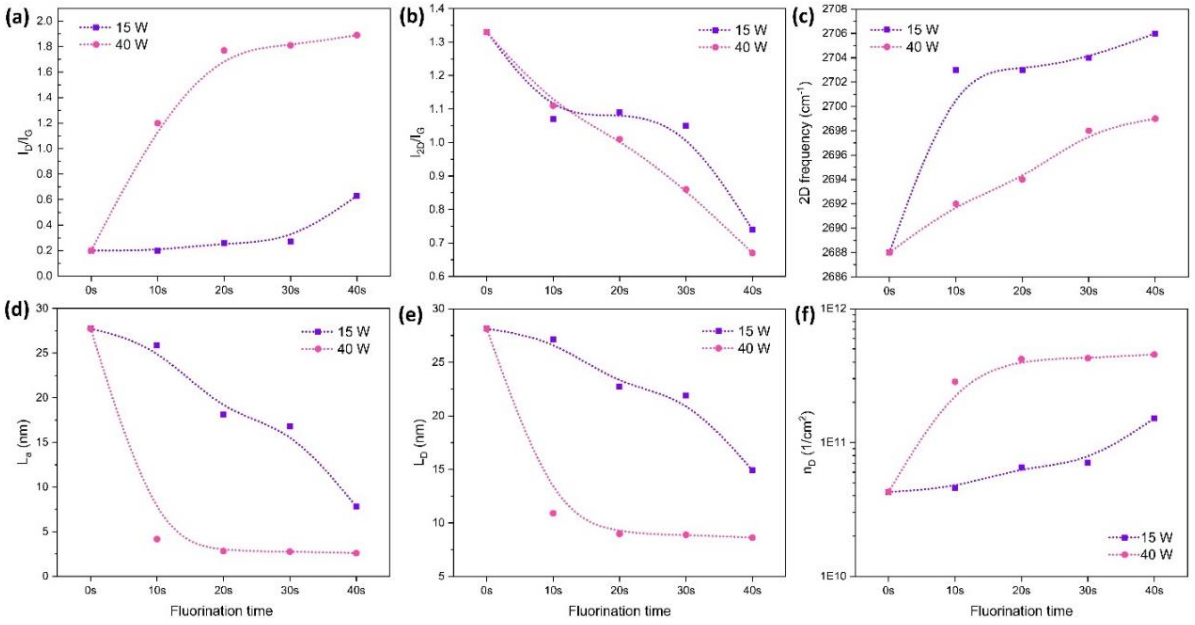

Fig. 5. a) ID/IG, b) I2D/IG, c) 2D frequency, d) L_a, e) average L_D and f) n_D variations with fluorination time in graphene samples at 0 s-40 s fluorination with 15 W and 40 W SF_6 plasma exposure, extracted from Raman spectra of fluorinated graphene samples; demonstrating increase in defects, decrease in crystallinity, blue shift in 2D peak, decrease in crystal domain, decrease in defect distance and increase in defect density of graphene samples with the increase in fluorination time

[DOI: 10.22068/ijmse.4004]

Table 1. 2D peak position, I_G/I_D, I_G/I_{2D} and L_a variations with fluorination time in graphene samples with 15 W and 40 W SF_6 plasma exposure data extracted from Raman spectra and compared with those in the relevant literature. Quantities with * are calculated from available data for better comparison

Plasma power	Plasma duration	Plasma type	λ(nm) laser	$I_{G/D}$	$I_{G/2D}$	L_a (nm)	L_D (nm)	n_D ($\frac{1}{cm^2}$)	Ref
0 W	0 s	SF_6	532	5.59	0.75	27.75	28.13	4.27e10	this work
15 W	10 s	SF_6	532	5.22	0.96	25.87	27.16	4.58e10	this work
	20 s	SF_6	532	3.66	0.92	18.15	22.75	6.53e10	this work
	30 s	SF_6	532	3.39	0.94	16.81	21.89	7.05e10	this work
	40 s	SF_6	532	1.58	1.37	7.82	14.93	1.52e11	this work
40 W	10 s	SF_6	532	0.84	0.9	4.16	10.89	2.84e11	this work
	20 s	SF_6	532	0.57	0.99	2.83	8.97	4.19e11	this work
	30 s	SF_6	532	0.56	1.17	2.77	8.89	4.28e11	this work
	40 s	SF_6	532	0.53	1.38	2.61	8.62	4.55e11	this work
40 W	10 s	CF_4	532	0.40	1.33	1.98*	-	-	[50]
50 W	120 s	CF_4	514	0.55	2.08	2.39*	-	-	[32]
10 W	5 min	CF_4	514	< 1	-	4.36*	-	1.00e14	[52]
-	5 min	CF_4	532	0.67	0.82	3.32*	8.58	-	[30]

3.4. Morphological and Elemental Aspects of Fluorination

Figure 6a demonstrates an SEM image of a large area of as-grown monolayer graphene on Cu by Graphenea with grain sizes of up to 20 μm, for the sake of comparison.

The enlarged area in Figure 6b shows the waviness of the underlying Cu surface and focuses on grain boundary intersections. The images were taken at 5 kV accelerating voltage and can be considered for a 0 W 0 s fluorination process. At 40 W plasma exposure of SF_6 to the graphene surface, various dark points are visible in the SEM images in Figure 6b where plasma time varies from 10s to 40 s. These dark regions were absent when no fluorination took place. There is also an evolution of the graphene surface with the increase in fluorination time at this power. These images were taken at equal magnification (2000 times) with 5 kV accelerating voltage. To gain more insight into the morphology changes of the graphene surface with fluorination, SEM images (in Figure 7) were taken on both 15 W and 40 W samples at 10 s-40 s for comparison, with a magnification of 5000 times and an accelerating voltage of 20 kV. Clearly, at 15 W, the evolution of the graphene surface is very mild, with very few dark points with respect to 40 W, highlighting the wavy structure of CVD graphene on Cu. SEM images obtained at a lower accelerating voltage in Figure 6 show much more details of the graphene surface than those obtained at a higher accelerating voltage in Figure 7 due to the penetration depth dependency of electron beams with accelerating voltage.

Figure 6c compares EDS spectra of a graphene sheet at 15 W and 40 W, both with 10 s fluorination, similar magnification and accelerating voltage. Both spectra demonstrate the presence of the underlying substrate Cu at around 8 keV and 8.9 keV. In an EDS spectrum, each element gives a peak at characteristic X-ray energies (keV), corresponding to specific electronic transitions known as K_α, K_β, L_α, etc. With the increase in plasma power, the intensity of the peak related to F increases as expected. The height/area of a peak in the EDS spectrum is proportional to the number of characteristic X-rays detected from that element. In studying EDS results, it is more important to investigate the relative weight (W%) and atomic (A%) percentages of the key elements we are after. Since the intensity of the peaks counts photons events, it does not directly represent W% or A%. Figure 6d illustrates quantitatively the evolution of F/C ratio in 15 W and 40 W samples at 10 s-40 s fluorination in two distinct magnifications and accelerating voltages of EDS. Additionally, EDS maps of F and C traces taken at both plasma power and individual plasma times in monolayer graphene samples are depicted in Figure 7. W% is the mass fraction of each element relative to the total sample mass. This tends to highlight heavier elements because they contribute more mass per atom. A% is the atomic fraction of each element relative to the total number of atoms. A heavier element with the same W% as a light element will show lower A%.

[DOI: 10.22068/ijmse.4004]

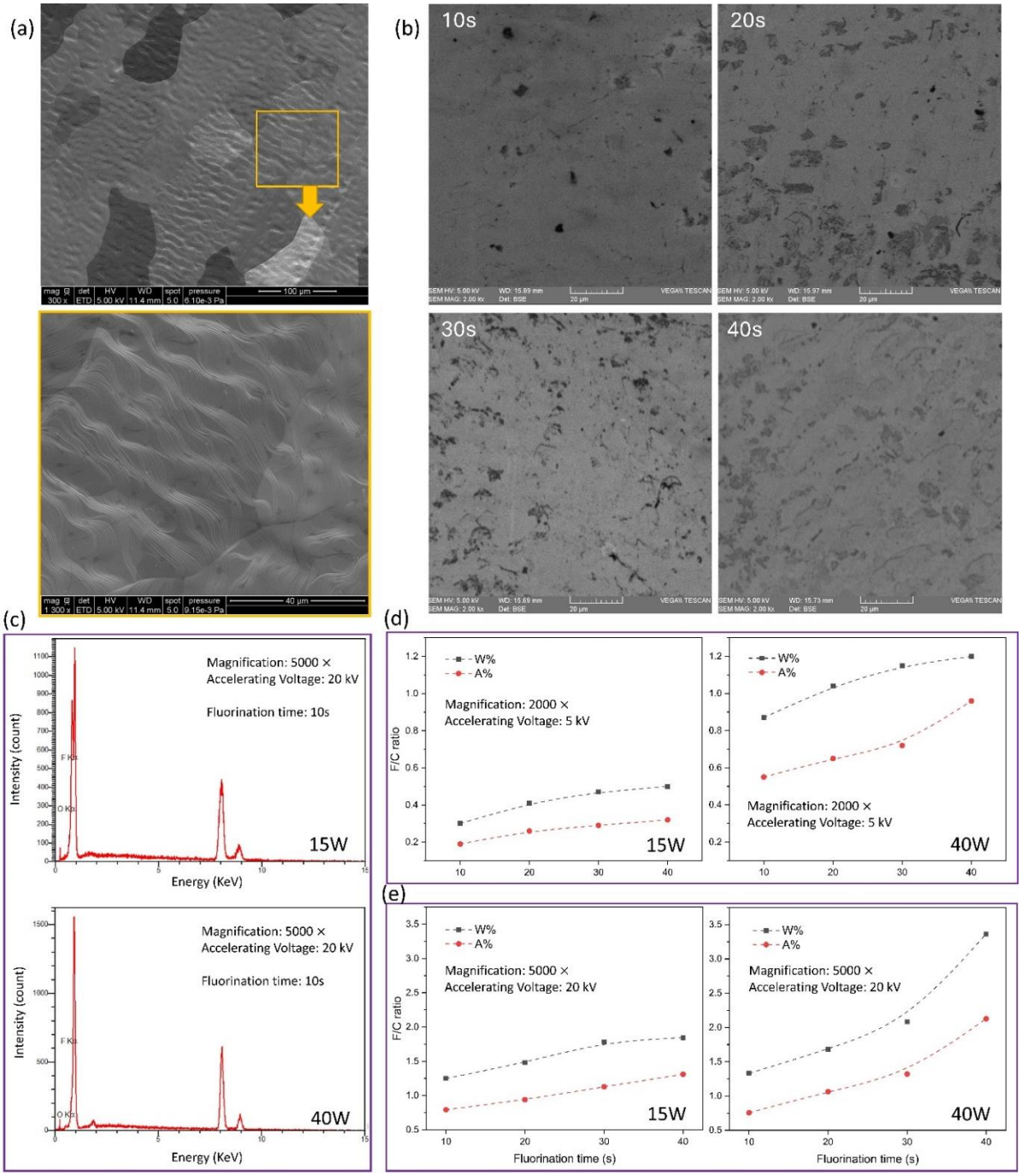

Fig. 6. a) SEM images of pristine as grown monolayer CVD graphene by Graphenea with large grain boundaries, with permission from Graphenea. b) SEM images of fluorinated graphene surface at 40 W in 0 s, 10 s, 20 s, 30 s and 40 s show an increase evolution of the surface with the increase in fluorination time at a constant plasma power. c) EDS spectra of fluorinated graphene at two plasma powers 15 W and 40 W, d,e) Fluorine/Carbon ratio comparison at two plasma powers 15 W and 40 W with fluorination time 0 s to 40 s with different EDS magnification, accelerating voltage and live time

In other words, for the same number of atoms, the heavier element contributes more to W%. With the increase in fluorination time (in Figure 7d), the F/C ratio increases in both plasma powers in great agreement with the Raman results and analyses. An increase in the F/C ratio (from 0.11 to 0.48) was mainly attributed to the formation of the CF–CF_2 group in a study conducted by Z. Wang [71]. Evidently, the increase in F/C in 40 W samples is faster than in 15 W samples. However,

[DOI: 10.22068/ijmse.4004]

A% in all cases is lower than W% since F (19 g/mol) is heavier than C (12 g/mol). It is important to note that the quantity of the F/C ratio at each individual plasma time obtained from EDS measurements contains artefacts, and a much more precise F/C ratio can only be obtained by X-ray photoelectron spectroscopy (XPS) measurements, where photo-electrons are collected by a detector mostly from the very top (<5nm) surface. In EDS, X-rays emitted from the surface and parts of the bulk of the sample are collected in the detector, and the interaction volume of the electron beam is much larger than the spot size, and the actual X-ray signal comes from a pear-shaped volume. The sample here is a monolayer of graphene, one atomically thin layer, decorated with fluorine over an 18 µm Cu. Furthermore, F K_α at 0.677 keV is in the soft X-ray region where the ionization cross-section is high. Therefore, it produces a large number of X-rays per incident electron. So even a thin layer of F can generate an intense, sharp peak compared to the weaker C K_α at 0.277 keV. Briefly, in EDS measurement over an atomically thin graphene sheet, C is under-detected. However, in this study, the trend of F/C ratio variation is in focus and F/C individual values are not significant to the results.

Looking closer at the data in Figures 7d and 7e, one will realise that EDS conditions likewise significantly impact the F/C ratio. At 2000 times magnification and 5 kV accelerating voltage, F/C in both sets of samples at 15 W and 40 W is relatively slow and does not exceed 1.2 in 40 W 40 s. Notably, increasing the magnification to 5000 and the accelerating voltage to 20 kV causes F/C to increase much faster, reaching approximately 3.5 at 40 W after 40 seconds. It is known that the scanning area or magnification in SEM-EDS can impact the composition measurements. As mentioned, the interaction volume of the electron beam is very large and extends hundreds of nm to a few µm deep depending on the accelerating voltage and sample density. So, a large scan area (low magnification) integrates signals from both surface and substrate over many microns.

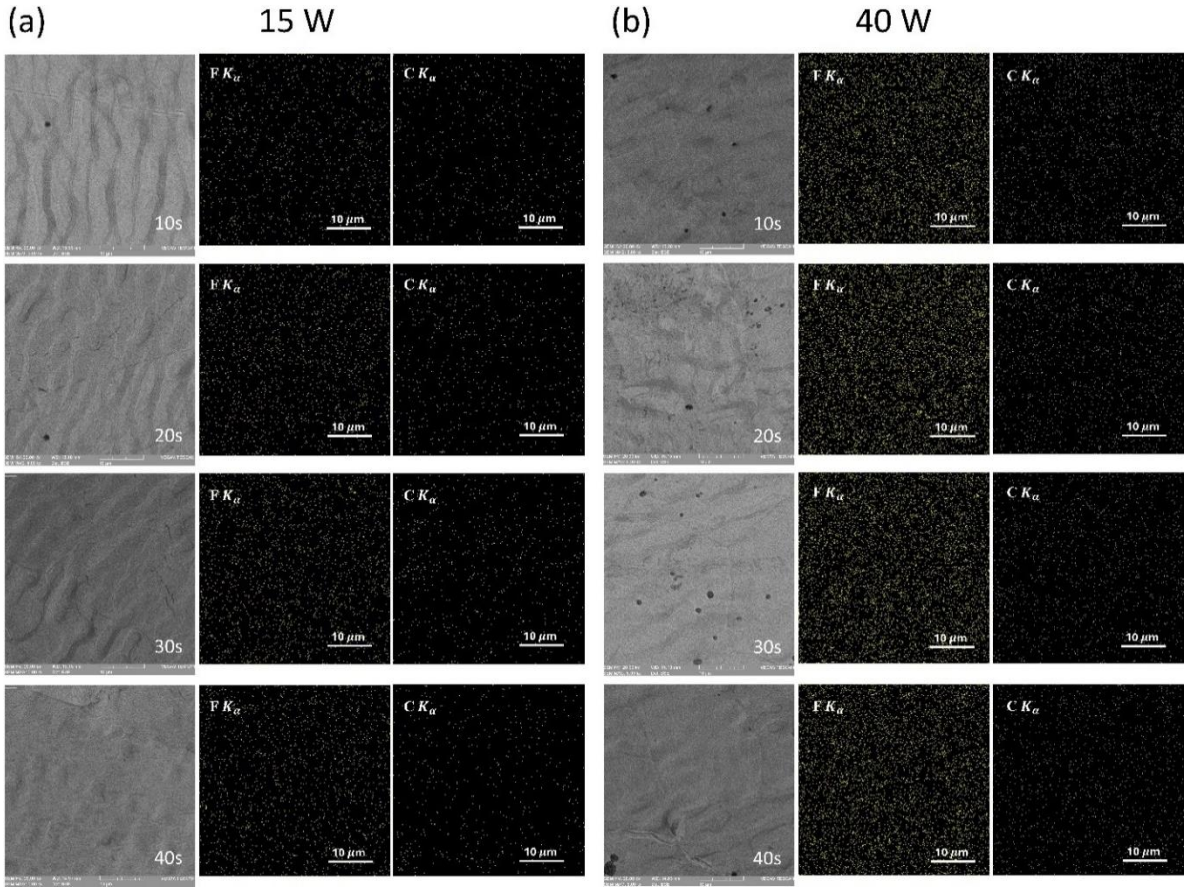

Fig. 7. SEM images along with F and C EDS map of fluorinated monolayer graphene a) at 15 W and b) at 40 W. All data taken with magnification of 5000 times and 20 kV accelerating voltage

[DOI: 10.22068/ijmse.4004]

Therefore, both F and C contributions are less significant, as seen in Figure 6d (with 2000 times magnification). A small scan area (high magnification) integrates signals more from the surface than the bulk so, the relative contribution of the fluorinated monolayer graphene becomes more significant. On the one hand, since F is detected more efficiently and C is under-detected, zooming in at higher magnifications removes some of the Cu background and makes the F/C ratio even higher. Briefly, the higher F/C ratios obtained in Figure 6e (with 5000 times magnification) are artefacts of sampling geometry and not an actual change in the composition of F or C atoms. EDS maps at 15 W and 40 W in Figure 7 also show a higher concentration of F with respect to C at both plasma powers, which relates to the same argument that C is under-detected.

4. CONCLUSIONS

Fluorinated graphene with its 2D layer-structure, high thermal and chemical stability, and other unique properties, may be adjusted via controlled fluorination processes, for a wide range of applications. In this work, monolayer CVD graphene grown on Cu was fluorinated with a time and power sequence trial via SF_6 plasma. To gain insight into the purity, roughness, adhesive forces, and wettability of fluorinated graphene. Structural, morphological, and elemental studies were carried out via SEM, EDS, and Raman spectroscopy along with surface roughness and adhesive force measurements via AFM. P-doped graphene was obtained upon fluorination, while a blue shift/red shift was observed in the 2D peak/D peak of the Raman spectra of fluorinated graphene. Lower plasma power (15W) at most fluorination times retained more graphene properties with respect to relevant studies in literature, having higher L_a, L_D and lower n_D, confirmed by Raman analyses. Surface roughness and adhesive forces on the graphene surface mainly were increased with the increase in plasma time at a certain power. Wettability tuning was observed in graphene samples that experienced varied fluorination time at both low and high plasma power, while, in contrast, samples fluorinated at higher plasma power exhibited more hydrophobicity, demonstrating how π-electron pairs play an essential role in tuning the wettability. SEM characterisations and EDS analyses showed more substantial surface evolution and a more significant increase of F/C for higher plasma power on the graphene sheet. EDS conditions also impacted on the F/C ratio, and the results were discussed accordingly. Overall, the results showed that lower plasma power retained more of the graphene properties while still demonstrating considerable tuning of the wettability with fluorination.

ACKNOWLEDGEMENT

The authors would like to thank Seyedeh Marzieh Hosseini for the useful discussions on EDS measurements.

REFERENCES

[1] Lu, X., Wang, X., Jin, J., Zhang, Q. & Chen, J. Electrochemical biosensing platform based on amino acid ionic liquid functionalized graphene for ultrasensitive biosensing applications. Biosens. Bioelectron., 2014, 62, 134–139.

[2] Zhang, J. , Lei, J. , Pan, R. , Xue, Y. & Ju, H. Highly sensitive electrocatalytic biosensing of hypoxanthine based on functionalization of graphene sheets with water-soluble conducting graft copolymer. Biosens. Bioelectron., 2010, 26, 371–376.

[3] Zhang J. et al., Hydrophilic, Clean Graphene for Cell Culture and Cryo-EM Imaging, Nano Lett., 2021, 21, 22, 9587–9593.

[4] Aghigh, A. et al. Recent advances in utilization of graphene for filtration and desalination of water: A review. Desalination, 2015, 365, 389–397.

[5] Han, Y., Xu, Z. & Gao, C. Ultrathin Graphene Nanofiltration Membrane for Water Purification. Adv. Funct. Mater., 2013, 23, 3693–3700.

[6] Mahmoud, K. A., Mansoor, B., Mansour, A. & Khraisheh, M. Functional graphene nanosheets: The next generation membranes for water desalination. Desalination, 2015, 356, 208–225.

[7] Kazemi, A.S., S.M. Hosseini, and Y. Abdi, Large total area membrane of suspended single layer graphene for water desalination. Desalination, 2019. 451: p. 160-171.

[8] Kazemi, A.S., et al., Support based novel

[DOI: 10.22068/ijmse.4004]

single layer nanoporous graphene membrane for efficacious water desalination. Desalination, 2019. 451: p. 148-159.
[9] Yin, J. et al. Generating electricity by moving a droplet of ionic liquid along graphene. Nat. Nanotechnol., 2014, 9, 378–383.
[10] Song, B. et al. Water-dispersible graphene/ polyaniline composites for flexible micro-supercapacitors with high energy densities. Nano Energy, 2015, 16, 470–478.
[11] Hong S.M. et al., Enhanced lithium-and sodium-ion storage in an interconnected carbon network comprising electronegative fluorine, ACS Appl. Mater. Interfaces, 2017, 9(22), 18790-18798.
[12] Wang, S. et al. High mobility, printable, and solution-processed graphene electronics. Nano let., 2009, 10 (1), 92-98.
[13] Liu Y., Li J., Chen X., Luo J., Fluorinated Graphene: A Promising Macroscale Solid Lubricant under Various Environments, ACS Appl. Mater. Interfaces 2019, 11, 43, 40470–40480.
[14] Carpenter J., Kim H., Suarez J., Zande A., Miljkovic N., The Surface Energy of Hydrogenated and Fluorinated Graphene, ACS Appl. Mater. Interfaces, 2023, 15, 1, 2429–2436.
[15] Prydatko, A.V. et al., Contact angle measurement of free-standing square-millimeter single-layer graphene. Nat. Commun., 2018, 9, 4185.
[16] Rafiee, J. et al. Wetting-Transparent Graphene Films for Hydrophobic Water-Harvesting Surfaces. Nature Mater., 2012, 11, 217–222.
[17] Belyaeva, L. A., van Deursen, P. M. G., Barbetsea, K. I. & Schneider, G. F. Hydrophilicity of graphene in water through transparency to polar and dispersive interactions. Adv. Mater., 2018, 30, 1–7.
[18] Taherian, F., Marcon, V., Van Der Vegt, N. F. A. & Leroy, F. What is the contact angle of water on graphene? Langmuir, 2013, 29, 1457–1465.
[19] Tian, Tian; Lin, Shangchao; Li, Siyu; Zhao, Lingling; Santos, Elton J. G.; Shih, Chih-Jen (2017). Doping-Driven Wettability of Two-Dimensional Materials: A Multiscale Theory. Langmuir, 2017, 33, 44, 12827–12837.
[20] Li, Z. et al. Effect of airborne contaminants on the wettability of supported graphene and graphite. Nat. Mater., 2013, 12, 925–931.
[21] Aria, A. I. et al. Time evolution of the wettability of supported graphene under ambient air exposure. J. Phys. Chem. C. 2016, 120, 2215–2224.
[22] Guo H. et al. On the Mechanism of Hydrophilicity of Graphene, Nano Lett. 2016, 16, 7, 4447–4453.
[23] Jangyup S. et al., Jongill, Tunable Wettability of Graphene through Nondestructive Hydrogenation and Wettability-Based Patterning for Bioapplications, Nano Lett., 2020, 20, 8, 5625–5631.
[24] M. Annamalai, K. Gopinadhan, S. A. Han, S. Saha, H. Park, E. B. Cho, B. Kumar, A. Patra, S. Kim and T. Venkatesan, Surface energy and wettability of van der Waals structures, Nanoscale, 2016, 8, 5764-5770.
[25] W. Feng, P. Long, Y. Feng, Y. Li, Two-Dimensional Fluorinated Graphene: Synthesis, Structures, Properties and Applications, Adv. Sci., 2016, 3, 1500413.
[26] R. R. Nair, W. Ren, R. Jalil, I. Riaz, V. G. Kravets, L. Britnell, P. Blake, F. Schedin, A. S. Mayorov, S. Yuan, M. I. Katsnelson, H. Cheng, W. Strupinski, L. G. Bulusheva, A. V Okotrub, I. V Grigorieva, A. N. Grigorenko, K. S. Novoselov, A. K. Geim, Fluorographene: A Two-Dimensional Counterpart of Teflon, Small, 2010, 6, 2877.
[27] Wang, H., Narasaki, M., Zhang, Z. et al. Ultra-strong stability of double-sided fluorinated monolayer graphene and its electrical property characterization. Sci Rep., 2020, 10, 17562.
[28] A. Ranjan, N. Raghavan, B. Liu, S. J. O. Shea, K. Shubhakar, C. S. Lai, K. L. Pey, IEEE Int. Reliab. Phys. Syposium, IEEE, Piscataway, NJ 2017, pp. 3C-5.1–3C-5.6.
[29] K. Ho, M. Boutchich, C. Su, R. Moreddu, E. Sebastian, R. Marianathan, L. Montes, C. Lai, A Self-Aligned High-Mobility Graphene Transistor: Decoupling the Channel with Fluorographene to Reduce Scattering, Adv. Mater., 2015, 27, 6519.
[30] Bo Liu, Ming-Chun Hong, Mamina Sahoo, Bin Leong Ong, Eng Soon Tok, MengFu Di, Yu-Ping Ho, Hanyuan Liang, Jong-Shing Bow, Zhiwei Liu, Jer-Chyi Wang, Tuo-Hung Hou, and Chao-Sung Lai, A

[DOI: 10.22068/ijmse.4004]

Fluorographene-Based Synaptic Transistor, Adv. Mater. Technol. 2019, 1900422.
[31] Li, D.; Xu, K.; Zhang, Y. A Review on Research Progress in Plasma-Controlled Superwetting Surface Structure and Properties. Polymers 2022, 14, 3759.
[32] Lim, T., Ju, S. Control of graphene surface wettability by using CF4 plasma. Surface & Coatings Technol. 2017, 328, 89-93.
[33] Slovin, Mitchell R, and Michael R. Shirts. Identifying Differences and Similarities in Static and Dynamic Contact Angles between Nanoscale and Microscale Textured Surfaces Using Molecular Dynamics Simulations. Langmuir, 2015, 31, 7980-7990.
[34] Kazemi, A.S., et al., Tuning wettability and surface order of MWCNTs by functionalization for water desalination. Desalination, 2021, 508, 115049.
[35] Huhtamäki, T.; Tian, X.; Korhonen, J. T.; Ras, R. H. A. Surface-wetting characterization using contact-angle measurements, Nature Protocols, 2018, 13, 1521–1538.
[36] Zahra Ebrahim Nataj, Asieh Sadat Kazemi, Yaser Abdi. "Surface effects and wettability measurement considerations in fluorinated carbon nanotubes", Appl. Phys. A, 2021, 127, 874.
[37] Saito, R.; Hofmann, M.; Dresselhaus, G.; Jorio, A.; Dresselhaus, M. S. Raman spectroscopy of graphene and carbon nanotubes, Advances in Physics, 2011, 60(3), 413-550.
[38] Dresselhaus M. S., Jorio A., Hofmann M., Dresselhaus G., Saito R.: Perspectives on carbon nanotubes and graphene Raman spectroscopy. Nano Letters, 2010, 10, 751–758.
[39] A. C. Ferrari & D. M. Basko, Raman spectroscopy as a versatile tool for studying the properties of graphene, Nat. Nanotech., 2013, 8, 235–246.
[40] A. C. Ferrari, J. Robertson, Interpretation of Raman spectra of disordered and amorphous carbon, Phys. Rev. B., 61 2000, 20, 14095.
[41] M. J. Mathews, M. A. Pimenta, G. Dresselhaus, M. S. Dresselhaus, M. Endo, Origin of dispersive effects of the Raman D band in carbon materials, Phys. Rev. B., 1999, 59 (10) R6585.
[42] Cançado, L. G.; Jorio, A.; Ferreira, E. H. Martins; Stavale, F.; Achete, C. A.; Capaz, R. B.; Moutinho, M. V. O.; Lombardo, A.; Kulmala, T. S.; Ferrari, A. C., Quantifying Defects in Graphene via Raman Spectroscopy at Different Excitation Energies, 2011, 11(8), 3190–3196.
[43] Tang, Bo; Guoxin, Hu; Gao, Hanyang, Raman Spectroscopic Characterization of Graphene. Applied Spectroscopy Reviews, 2010, 45(5), 369–407.
[44] Zheng, Xiaoming; Chen, Wei; Wang, Guang; Yu, Yayun; Qin, Shiqiao; Fang, Jingyue; Wang, Fei; Zhang, Xue-Ao, The Raman redshift of graphene impacted by gold nanoparticles. AIP Advances, 2015, 5(5), 057133–7.
[45] Ferrante, C., Virga, A., Benfatto, L. et al. Raman spectroscopy of graphene under ultrafast laser excitation. Nat Commum., 2018, 9, 308.
[46] Calizo, I., Miao, F., and Lau, C.N., Variable temperature Raman microscopy as a nanometrology tool for graphene layers and graphene-based devices. Appl. Phys. Lett., 2007, 91, 071913–071915.
[47] Zhen, H.N., Hao, M.W., and Yun, M. Tunable stress and controlled thickness modification in graphene by annealing. ACS Nano., 2008, 2, 1033–1039.
[48] Jiang-Bin Wu, Miao-Ling Lin, Xin Cong, He-Nan Liu and Ping-Heng Tan, Raman spectroscopy of graphene-based materials and its applications in related devices, Chem. Soc. Rev., 2018, 47, 1822-1873.
[49] Zhang, H.; Fan, L.; Dong, H.; Zhang, P.; Nie, K.; Zhong, J.; Li, Y.; Guo, J.; Sun, X. Spectroscopic Investigation of Plasma-Fluorinated Monolayer Graphene and Application for Gas Sensing. ACS Appl. Mater. Interfaces, 2016, 8, 8652–866.
[50] Cheng, L.; Jandhyala, S.; Mordi, G.; Lucero, A. T.; Huang, J.; Azcatl, A.; Wallace, R. M.; Colombo, L.; Kim, J. Partially Fluorinated Graphene: Structural and Electrical Characterization. ACS Appl. Mater. Interfaces, 2016, 5002–5008.
[51] Tahara, K.; Iwasaki, T.; Matsutani, A.; Hatano, M. Effect of Radical Fluorination on Mono and Bi-Layer Graphene in Ar/F_2 Plasma. Appl. Phys. Lett., 2012, 101, 163105.
[52] Bei Wang, Junjie Wang, Jun Zhu, Fluorination of Graphene: A Spectroscopic

[DOI: 10.22068/ijmse.4004]

and Microscopic Study, ACS Nano, 2014, 8, 2, 1862–1870.
[53] Bakharev, P.V., Huang, M., Saxena, M. et al. Chemically induced transformation of chemical vapour deposition grown bilayer graphene into fluorinated single-layer diamond. Nat. Nanotechnol. 2020, 15, 59–66.
[54] Ho, KI., Huang, CH., Liao, JH. et al. Fluorinated Graphene as High Performance Dielectric Materials and the Applications for Graphene Nanoelectronics. Sci Rep. 2014, 4, 5893.
[55] Ali Ashraf, Yanbin Wu, Michael Cai Wang, Keong Yong, Tao Sun, Yuhang Jing, Richard T. Haasch, Narayana R. Aluru, and SungWoo Nam, Doping-Induced Tunable Wettability and Adhesion of Graphene, Nano Lett. 2016, 16, 7, 4708–4712.
[56] Demetrios D. Chronopoulos, Aristides Bakandritsos, Martin Pykal, Radek Zbořil, Michal Otyepka, Chemistry, properties, and applications of fluorographene, Applied Materials Today, 2017, 9, 60-70.
[57] C. Lee, X. D. Wei, J. W. Kysar, J. Hone, Measurement of the Elastic Properties and Intrinsic Strength of Monolayer Graphene, Science, 2008, 321, 385.
[58] Tian, Tian; Lin, Shangchao; Li, Siyu; Zhao, Lingling; Santos, Elton J. G.; Shih, Chih-Jen (2017). Doping-Driven Wettability of Two-Dimensional Materials: A Multiscale Theory. Langmuir, 2017, 33, 44, 12827–12837.
[59] Hong, Guo; Han, Yang; Schutzius, Thomas M.; Wang, Yuming; Pan, Ying; Hu, Ming; Jie, Jiansheng; Sharma, Chander S.; Müller, Ulrich; Poulikakos, Dimos (2016). On the Mechanism of Hydrophilicity of Graphene, Nano Lett. 2016, 16, 7, 4447–4453.
[60] Presel, Francesco; Gijón, Alfonso; Hernández, Eduardo R.; Lacovig, Paolo; Lizzit, Silvano; Alfè, Dario; Baraldi, Alessandro (2019). Translucency of Graphene to van der Waals Forces Applies to Atoms/Molecules with Different Polar Character, ACS Nano, 2019, 13, 10, 12230–12241.
[61] Gun-Tae Kim, Su-Ji Gim, Seung-Min Cho, Nikhil Koratkar, Il-Kwon Oh, Wetting-Transparent Graphene Films for Hydrophobic Water-Harvesting Surfaces, Adv. Mater. 2014, 26 (30), 5166-5172.
[62] Liao CD, Capasso A, Queirós T, Domingues T, Cerqueira F, Nicoara N, Borme J, Freitas P, Alpuim P. Optimizing PMMA solutions to suppress contamination in the transfer of CVD graphene for batch production. Beilstein J Nanotechnol. 2022, 18 (13), 796-806.
[63] Seonyeong Kim, Somyeong Shin, Taekwang Kim, Hyewon Du, Minho Song, ChangWon Lee, Kisoo Kim, Seungmin Cho, David H. Seo, Sunae Seo, Robust graphene wet transfer process through low molecular weight polymethylmethacrylate, Carbon, 2016, 98, 352-357.
[64] Grzegorx Lupina et al. Residual Metallic Contamination of Transferred Chemical Vapor Deposited Graphene, ACS Nano 2015, 9, 5, 4776–4785.
[65] Ochedowski, O., Bussmann, B. & Schleberger, M. Graphene on Mica-Intercalated Water Trapped for Life. Sci Rep (2014) 4, 6003.
[66] Fan Yang, Grzegorz Stando, Annette Thompson, Dhruthi Gundurao, Lei Li, Haitao Liu, Effect of Environmental Contaminants on the Interfacial Properties of Two-Dimensional Materials, Acc. Mater. Res. 2022, 3, 10, 1022–1032.
[67] Chronopoulos, D. D.; Bakandritsos, A.; Lazar, P.; Pykal, M.; Čépe, K. r.; Zbořil, R.; Otyepka, M. High-yield alkylation and arylation of graphene via grignard reaction with fluorographene. Chem. Mater. 2017, 29 (3), 926-930.
[68] Bakandritsos, A.; Pykal, M.; Błoński, P.; Jakubec, P.; Chronopoulos, D. D.; Poláková, K. i.; Georgakilas, V.; Cepe, K.; Tomanec, O.; Ranc, V. Cyano graphene and graphene acid: emerging derivatives enabling high-yield and selective functionalization of graphene. ACS Nano. 2017, 11 (3), 2982-2991.
[69] S.Y. Misyura, V.A. Andryushchenko, V.S. Morozov, The effect of temperature on the contact angle of a water drop on graphene and graphene synthesized on copper, Materials Science and Engineering: B, 2023, 290, 116341.
[70] Jia-Wen Song, Li-Wu Fan, Temperature dependence of the contact angle of water: A review of research progress, theoretical understanding, and implications for boiling heat transfer, Advances in Colloid and

[DOI: 10.22068/ijmse.4004]

Interface Science, 2021, 288, 102339.
[71] Z. Wang, J. Wang, Z. Li, P. Gong, X. Liu, L. Zhang, J. Ren, H. Wang, S. Yang, Synthesis of fluorinated graphene with tunable degree of fluorination, Carbon, 2012, 50, 5403.

[DOI: 10.22068/ijmse.4004]